

Emission of time-ordered photon pairs from a single polaritonic Bogoliubov mode

Ferdinand Claude,^{1,2} Yueguang Zhou,^{1,2} Sylvain Ravets,³ Jacqueline Bloch,³ Martina Morassi,³ Aristide Lemaître,³ Alberto Bramati,⁴ Anna Minguzzi,⁵ Iacopo Carusotto,⁶ Irénée Frérot,⁴ and Maxime Richard^{1,2}

¹*Majulab International Research Laboratory, French National Centre for Scientific Research, National University of Singapore, Nanyang Technological University,*

Sorbonne Université, Université Côte d'Azur, 117543 Singapore

²*Centre for Quantum technologies, National University of Singapore, 117543 Singapore*

³*Université Paris-Saclay, CNRS, Centre de Nanosciences et de Nanotechnologies, 91120 Palaiseau, France*

⁴*Laboratoire Kastler Brossel, Sorbonne Université, CNRS,*

ENS-PSL Research University, Collège de France, 4 Place Jussieu, 75005 Paris, France

⁵*Univ. Grenoble Alpes, CNRS, LPMMC, 38000 Grenoble, France*

⁶*Pitaevskii BEC Center, INO-CNR and Dipartimento di Fisica, Università di Trento, via Sommarive 14, I-38123 Trento, Italy*

In many-body quantum systems, interactions drive the emergence of correlations that are at the heart of the most intriguing states of matter. A remarkable example is the case of weakly interacting bosonic systems, whose ground state is a squeezed vacuum state, and whose elementary excitations have a collective nature. In this work, we report on the direct observation of the peculiar microscopic quantum structure of these elementary excitations. We perform time- and frequency-resolved two-photon correlation measurements on the fluctuations of weakly interacting polaritons in a resonantly-driven microcavity, and observe that upon decreasing the average number of fluctuation quanta below unity, large pair correlations build up together with strong time-ordering of the emitted photons. This behavior is a direct signature of the particle-hole quantum superposition which is at the heart of Bogoliubov excitations.

Early on, the observation of two-photon correlation has been crucial in characterizing and understanding quantum states of light. This began with the pioneering work of Hanbury-Brown and Twiss, who used two-photon correlations in thermal light to improve the angular resolution in astronomical measurements [1], and with the characterization of quantum indistinguishability of two identical photons, using Hong-Ou-Mandel two-photon interferences [2]. With the experimental realization of effective two-level systems like single atoms or quantum dots, two-photon correlation measurements have been used extensively to understand their dynamics and the deeply-quantum states of light that they can generate, such as Fock states and other more sophisticated few-photon states [3–7]. In systems of interacting particles, the dynamics can get even richer and more complex, leading to the emergence of a large variety of macroscopic quantum phenomena involving many-body correlations, such as superfluid-insulator phase transition [8], fermionization of bosons [9–12], or fractional quantum Hall states in ultracold atoms [13–15] and photonic systems [16–19].

Quite remarkably, the emergence of rich correlations

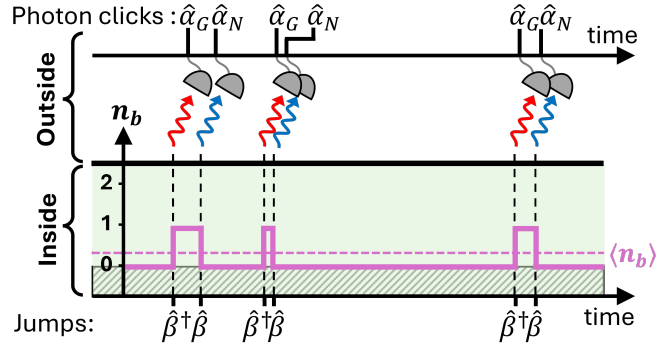


FIG. 1. Mechanism of time-ordering in the correlated photon pairs emitted by a single Bogoliubov mode – Qualitative sketch of the time-evolution of the number of excitation quanta n_b in a single mode Bogoliubov field (purple thick line), in the regime $\langle \hat{n}_b \rangle = \langle \hat{\beta}^\dagger \hat{\beta} \rangle < 1$. The Bogoliubov field leaks outside the system by emitting photons across the imperfect mirrors (horizontal black thick line). Every time a normal [ghost] photon is detected ("photon clicks"), the Bogoliubov field $\hat{\beta}$ is projected ("Jumps") into a state with one less [one more] excitation. Normal (ghost) photons are shown in blue (red) wavy arrows, and the corresponding operator $\hat{a}_N \propto \hat{a}_N$ ($\hat{a}_G \propto \hat{a}_G$) is mentioned for each photon click event.

also occurs in dilute bosonic systems characterized by weak interactions, in which a small fluctuating fraction of the system involves quantum mechanically nontrivial elementary excitations with a collective nature described by the celebrated Bogoliubov theory [20, 21]. This theory captures paradigmatic macroscopic phenomena in these systems, such as the emergence of superfluidity in ultracold atomic condensate [22] and photonic systems [23], and the quantum depletion of the condensate even at vanishing temperature [24]. In spite of its relative simplicity, the cornerstone of Bogoliubov theory is an intriguing quantum structure which is rooted in the very nature of the elementary excitation : a quantum superposition of the creation and annihilation of an excited particle out of the coherent condensate, sometimes equivalently described as a particle and hole superposition [21].

This structure is formally expressed by the Bogoliubov transformation $\hat{\beta}^\dagger = u\hat{a}^\dagger - v\hat{a}$, where \hat{a}^\dagger and $\hat{\beta}^\dagger$ are respectively the particle and Bogoliubov-excitation creation operators, and (u, v) are the Bogoliubov coefficients. In particular, it leads to the emergence of a negative-frequency density-of-state in the excitation spectrum (the so-called Ghost modes), as observed in ultracold atom systems [22, 25] and in quantum fluids of light [26–29], and to two-body correlations between atoms of opposite momenta picked up within the quantum depleted fraction of a weakly interacting ultra-cold atom condensate, as recently observed in [30]. Nevertheless, the fundamental quantum structure of Bogoliubov excitations has a unique physical meaning which goes beyond what is captured by these observables alone. Fundamentally, the hybridization of the creation and annihilation processes opens up the possibility to observe – via time- and frequency-resolved two-photon correlation measurements – both the addition *and* subtraction of an excitation quantum in the Bogoliubov fluctuation field. As we show in this work, this feature results in non-trivial time-ordering of the detected particles whenever the average excitation number of the Bogoliubov field is smaller than one. In this work we take advantage of the high flexibility provided by Bogoliubov states of light [28, 29] to demonstrate the occurrence of this unique time-ordered correlation.

PHYSICAL PRINCIPLE AND THEORY

In this section, we consider an idealized version of our experimental system: a photonic resonator featuring a single spatial mode (i.e. a micrometer-scale cavity), and containing a field of weakly interacting photons, and examine theoretically the quantum dynamics of the elementary excitations surrounding the coherent fraction of the field. In the Bogoliubov theory, the Hamiltonian describing the elementary excitations is that of a harmonic oscillator: $H = \hbar\omega_0\hat{\beta}^\dagger\hat{\beta}$, where ω_0 is the Bogoliubov excitation frequency. Using the Bogoliubov transformation, assuming a small dissipation rate $\kappa \ll \omega_0$, the corresponding intracavity photon dynamics can be derived from the Heisenberg equation as $\hat{a}(t) \simeq u\hat{\beta}e^{-i\omega_0 t} + v\hat{\beta}^\dagger e^{i\omega_0 t}$, which Fourier transforms into $\tilde{a}(\omega) = u\hat{\beta}\delta(\omega - \omega_0) + v\hat{\beta}^\dagger\delta(\omega + \omega_0)$.

Experimentally-relevant observables are based on the photons emitted by the system into the extracavity continuum (of operator $\hat{a}(t)$), that are weakly coupled to the intracavity field $\hat{a}(t)$ via the linear input-output relation $\hat{a}(t) = \hat{a}_{\text{in}}(t) - i\sqrt{\kappa}\hat{a}(t)$, where $\hat{a}_{\text{in}}(t)$ describe the input extracavity photon vacuum fluctuations. $\hat{a}_{\text{in}}(t)$ does not contribute to the photo-counting observables relevant to our work, and can be simply ignored, so that in practice we can use that $\hat{a}(t) \propto \hat{a}(t)$. Note that this derivation is also appropriate for the case in which photons are dressed with electron-hole pairs into exciton-polaritons

as in the experimental section presented later, provided that κ is simply corrected by the photonic Hopfield coefficients [31].

For the correlations that we are interested in, we consider two detectors of extracavity photons, each with a narrow frequency bandwidth acceptance $\Gamma_{bw} \ll \omega_0$, such that the first one detects only photons emitted at frequency ω_0 , and the second one only photons at $-\omega_0$, where these frequencies are given as relative to the mean-field one. At these two frequencies, the previous expression yields

$$\hat{a}(\omega_0) = u\hat{\beta} \equiv \hat{a}_N \quad (1)$$

$$\hat{a}(-\omega_0) = v\hat{\beta}^\dagger \equiv \hat{a}_G, \quad (2)$$

where $\hat{a}(\omega_0) = \int_{\omega_0 \pm \Gamma_{bw}/2} d\omega' \tilde{a}(\omega')$, and $\hat{a}_N \propto \hat{a}_N$ and $\hat{a}_G \propto \hat{a}_G$ are defined as the *Normal* and *Ghost* photons operators. This simple analysis shows that the detection of a Normal (Ghost) photon is an unambiguous witness of the fact that a quantum of excitations has been subtracted (added) to the Bogoliubov field. This correspondence is illustrated in the quantum trajectory spirit in Fig.1, where $n_b(t)$ is a stochastic Bogoliubov field trajectory in the Fock state ladder (vertical axis).

From there, we can derive a clear physical picture of the correlations between the Normal and Ghost photons. Using the fact that $\hat{a} \propto \hat{a}$, the normalized correlation of a normal-ghost emitted-photon pair in which the Normal photon is emitted first reads $\mathcal{G}_{NG}^{(2)} = \langle \hat{a}_N^\dagger \hat{a}_G^\dagger \hat{a}_G \hat{a}_N \rangle / (n_G n_N) \propto \langle \hat{\beta}^\dagger \hat{\beta} \hat{\beta}^\dagger \hat{\beta} \rangle$, while the one in which the Ghost photon is emitted first reads $\mathcal{G}_{GN}^{(2)} = \langle \hat{a}_G^\dagger \hat{a}_N^\dagger \hat{a}_N \hat{a}_G \rangle / (n_G n_N) \propto \langle \hat{\beta} \hat{\beta}^\dagger \hat{\beta} \hat{\beta}^\dagger \rangle$. Here, $n_{G,N} \equiv \langle \hat{a}_{G,N}^\dagger \hat{a}_{G,N} \rangle$ is the number of Ghost/Normal photons.

This correspondence means that, as illustrated in the Bogoliubov field trajectory represented in Fig.1, the first correlation measures the occurrence of a stochastic transient suppression of one elementary excitation from the field, i.e. a \cup -shaped excursion of the Bogoliubov excitation number, while the second corresponds to a stochastic transient addition of one elementary excitation to the field, i.e. a \cap -shaped excursion of the excitations number. The magnitude of these correlations can be simply expressed as a function of the Bogoliubov excitation number $n_b = \langle \hat{\beta}^\dagger \hat{\beta} \rangle$ as

$$\mathcal{G}_{NG}^{(2)} \simeq 1 + \frac{n_b}{1 + n_b} \quad (3)$$

$$\mathcal{G}_{GN}^{(2)} \simeq 1 + \frac{1 + n_b}{n_b}, \quad (4)$$

where we have assumed that the photon field is in a Gaussian state and $\langle \hat{\beta} \hat{\beta} \rangle \propto \gamma / (2\omega_0) \simeq 0$ (see SM section II). One can then distinguish two regimes. When $n_b \gg 1$ the quantization of the Bogoliubov fluctuation is irrelevant and the correlations are not time-ordered and converge to $\mathcal{G}_{GN}^{(2)} = \mathcal{G}_{NG}^{(2)} = 2$. The regime $n_b < 1$ (which occurs when the input rate of external noise coupled to the system is smaller than the cavity loss rate) is

the most interesting. This regime is illustrated in Fig.1: owing to the rarity of the fluctuations, and to the high probability of the system to be found in the ground state $|n_b = 0\rangle$, the excursion \cup is strongly suppressed, while \cap involves maximal correlations. This is directly visible in Eqs.(3,4) where $\mathcal{N}\mathcal{G}_{NG}^{(2)}$ tends to one for small n_b , while $\mathcal{G}_{GN}^{(2)}$ diverges. Physically, it means that when $n_b = 0$, the emission of a Normal photon is always preceded by the emission of a Ghost photon, while the emission of a Ghost photon carries no information on the prior emission of a normal photon. As discussed later on, this feature is in stark contrast with typical implementations of spontaneous parametric emission.

In order to achieve a quantitative understanding for our measurement of Normal-Ghost photon pair correlation versus delay τ , we expand these theoretical arguments into an input-output theory that consistently accounts for the system coupling to the outside photon modes via the decay rate γ_b of the Bogoliubov mode ($\gamma_b = \kappa$ except in specific conditions irrelevant here), and for the time dependence of the correlations, characterized by a tradeoff between delay and frequency resolution (see SM section II for a detailed derivation).

The frequency resolution is accounted for by considering that each detector has a spectrally-dependent response function $f_r(\omega)$ characterized by its bandwidth Γ_{bw} and central transmission frequency ω_r , such that the input-output relation becomes $\hat{a}_r(\tau) = \hat{a}_{in}(\tau) - i\sqrt{\kappa} \int_{-\infty}^{\tau} dt \tilde{f}_r(\tau - t) \hat{a}(t)$, where $\tilde{f}_r(t) = e^{-i\omega_r t} e^{-\Gamma_{bw} t}$ is the response function in the time domain. The Normal-Ghost photon coincidence rate can thus be expressed as:

$$I_{NG}^{(2)}(\tau) = \left\langle \mathcal{T}_-[\hat{a}_N^\dagger(0)\hat{a}_G^\dagger(\tau)]\mathcal{T}_+[\hat{a}_G(\tau)\hat{a}_N(0)] \right\rangle, \quad (5)$$

where \mathcal{T}_+ (resp. \mathcal{T}_-) orders the $a(t)$ operators with the latest time on the left (resp. right) [32].

Assuming as before a gaussian states for the photon field, and in the limit where $\langle \hat{\beta} \hat{\beta} \rangle \simeq 0$, and $\omega_0 \gg (\Gamma_{bw}, \gamma_b)$, the resulting Normal-Ghost correlation function $g_{NG}^{(2)}(\tau) = I_{NG}^{(2)}(\tau)/[I_N I_G]$ can be derived explicitly as

$$g_{NG}^{(2)}(\tau) = 1 + A \frac{\Gamma_{bw}^2}{(\Gamma_{bw} - \gamma_b)^2} \times \left[(1 - s_\tau \xi) e^{-\gamma_b |\tau|} - \left(\frac{\gamma_b}{\Gamma_{bw}} - s_\tau \xi \right) e^{-\Gamma_{bw} |\tau|} \right]^2, \quad (6)$$

where

$$A = 1 + [4n_b(n_b + 1)]^{-1} \quad (7)$$

$$\xi = (2n_b + 1)^{-1}. \quad (8)$$

In this expression, A is the characteristic amplitude of the correlation, ξ fixes the asymmetry of the correlation peak, and s_τ is the sign of τ , chosen such that correlation events in which the ghost photon is detected first correspond to $\tau < 0$. In this input-output model, the Normal-Ghost

photons time ordering is encoded in the parameter ξ : a value $\xi = 0$ means no time-ordering asymmetry, while $\xi = 1$ corresponds to the largest preference for ghost photon first. Consistently, in the regime where $\omega_0 \gg \Gamma_{bw} \gg \gamma_b$, and for Normal-Ghost photons delays $\Gamma_{bw}^{-1} \ll \tau \ll \gamma_b^{-1}$, $g_{NG}^{(2)}(\tau)$ matches $\mathcal{G}_{NG}^{(2)}$ for $\tau > 0$ and $\mathcal{G}_{GN}^{(2)}$ for $\tau < 0$. Note also that Eq.(6) does not depend on the mode spatial pattern, as it cancels out.

Importantly, this expression depends only on n_b , and not on the origin of the microscopic processes populating n_b , namely: the coupling to the extra-cavity vacuum [33], the thermal solid-state phonons that couple to polariton via their excitonic fraction [29], or the electronic noise [34]. Like in the simpler model of (3,4), the key feature of this expression is that $g_{NG}^{(2)}(\tau)$ becomes increasingly asymmetric, i.e. time-ordered, for decreasing $n_b \leq 1$, and correspondingly its peak magnitude increases, approximately as $(n_b + 1)/n_b$. Within this model, these two observables are locked to each other by the universal formula

$$A = (1 - \xi^2)^{-1}. \quad (9)$$

TIME-ORDERED CORRELATIONS MEASUREMENTS

The experiment is carried out within a spatially-confined micropillar microcavity of $7\ \mu\text{m}$ diameter, that features discrete transverse cavity mode resonances, and in which the photons are dressed by electron-hole pairs (excitons) into exciton-polaritons [31] in order to achieve sizable two-body interactions (cf. Methods section A for details on the system). The microcavity is cooled in a variable temperature cryostat at $T = [4, 10]\ \text{K}$ to stabilize and minimize the excitonic damping rate, and driven using a CW laser focused into a Gaussian spot of $4\ \mu\text{m}$ diameter on the surface of the microcavity top mirror.

We first record a spatially-resolved photoluminescence spectrum $I_{pl}(\omega, x)$ at $T = 4\ \text{K}$ in order to establish the system spectral properties. It is obtained under a very low non-resonant excitation to minimize the nonlinearities. The result is shown in Fig.2.a and shows two sets of discrete modes: the upper (UP) and lower (LP) polariton sets, as expected in polaritonic microcavities. The lowest energy (LP) transverse modes are spectrally-narrow and well separated from each other. The x -coordinate corresponds to a cross-section along the micropillar diameter. The energy $\hbar\omega_j$ and spatial patterns of each mode, as observed in $I_{pl}(x, \omega_j)$, are found to be in quantitative agreement with a model of cylindrically confined microcavity in the strong coupling regime (white and pink dashes and mode labels in Fig.2.a), which is outlined in the Method section B1.

We then drive a coherent polaritonic field in the LP 1s mode by tuning the laser $\hbar\delta_{las} = \hbar\omega_{las} - \hbar\omega_{lp,1s} = 90\ \mu\text{eV}$ above the 1s lower polariton mode resonance. Owing to the interactions, the system jumps up into resonance, and into a stable high-intensity field state that exhibits the

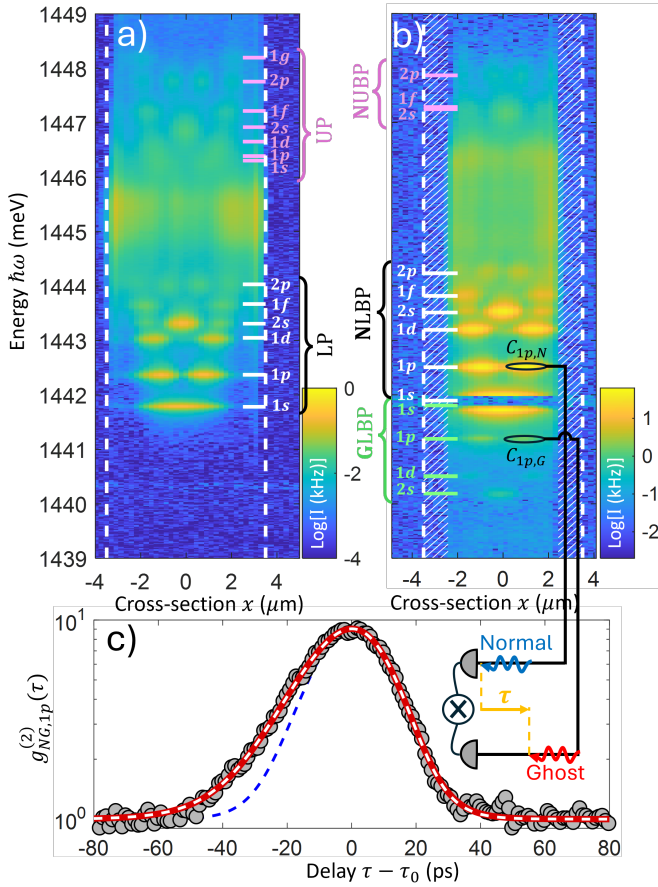


FIG. 2. **Measurement of time-ordered correlations between normal and ghost photons in a $7\mu\text{m}$ micropillar microcavity** Spatially-resolved photoluminescence spectroscopy $I_{PL}(x, \omega)$ in the low-intensity regime (a), and spatially-resolved emission spectrum of the fluctuation $I_b(x, \omega)$ under a strong resonant CW drive on the $1s$ LP mode (b). The photon count rate is plotted in logarithmic color scale. The micropillar edges are shown as vertical dashed lines. In b), an additional spatial filter rejects the emission from the micropillars edges (cross hatched region). The calculated micropillar lower (LP) and upper (UP) polariton levels in the linear regime are shown in (a) with their mode labels as white and pink dashes respectively. The calculated Bogoliubov normal-UP (NUBP), normal-LP (NLBP) and ghost-LP (GLBP) modes are shown in (b) with their mode labels as pink, white and green dashes respectively. The single photon collection areas used for the detection of the normal (ghost) photon $C_{N,1p}$ ($C_{G,1p}$) in the correlation measurement are indicated in b). The vertical (horizontal) size of $C_{N(G),1p}$, the collected regions, indicates the collected spectral bandwidth $\hbar\Gamma_{bw}$ (the horizontal extension Δx of the collected mode area). (c) Measured (round symbols) normal-ghost photon correlation function $g_{NG,1p}^{(2)}(\tau)$. $\tau_0(\omega_{N,G}) \in [-15, 15]$ ps is a small unknown delay offset due to optical path length dependence on $\omega_{N,G}$. The thick red, and dashed white lines are fits to the data obtained using the Bogoliubov model Eq.(6), and the relaxed lineshape model respectively. The latter is also obtained from Eq.(6), but A and ξ are left independent. τ_0 is a fixed offset determined by the fit with the Bogoliubov model. The blue dashed line is a fit of the right side ($\tau \geq 0$), using a the relaxed lineshape model and taking $\xi = 0$ (symmetric peak).

desired Bogoliubov regime of weak but not negligible interactions: $gn_0 \simeq \delta_{las} > \hbar\gamma_{lp,1s}$, where $\hbar\gamma_{lp,1s} = 45\mu\text{eV}$ is the LP $1s$ mode linewidth, gn_0 is the internal interaction energy, where g is the interaction constant and n_0 is the number of intracavity polaritons. Note that we avoid tuning the system parameters into the bistable window, in which the system is bistable [31], and the high intensity field state is thus unstable over the integration time.

Like in spatially-extended two-dimensional systems [29], we can filter out the dominant mean-field emission and characterize the spectral properties of the Bogoliubov excitations. An example of spatially-resolved emission spectrum $I_b(\omega, x)$ measured in this way is shown in Fig.2.b. We observe discrete emission lines, where the positive (negative) energies $\omega_b > \omega_{las}$ ($\omega_b < \omega_{las}$) correspond to Normal (Ghost) Bogoliubov components. These spectral lines are well resolved within the Normal and Ghost Lower Bogoliubov polariton (labeled NLBP and GLBP in Fig.2.b) energy ranges (involving the $1s$, $1p$, $1d$ and $2s$ modes; parameters in the caption). The Upper Bogoliubov polariton modes are much blurrier but do not play any role in this work. We check that the obtained spectra are consistent with the Bogoliubov excitation picture, by running a numerical simulation of Bogoliubov levels in a multi-mode driven-dissipative cylindrical micropillar microcavity. The calculated levels are shown as color dashes and labels in Fig.2.b, and found to be in excellent agreement with the measurement (cf details in Methods section B 2).

We then measure the normalized correlations $g_{NG,1p}^{(2)}(\tau)$ between the Normal and Ghost photons emitted by the Bogoliubov excitations in mode $1p$. To do so, we select two small collection areas $C_{1p,N}$ and $C_{1p,G}$ (indicated by the two black ellipses in Fig.2.b) in the spectrally- and spatially-resolved detection focal plane where the emission pattern $I_b(\omega, x)$ of Fig.2.b is formed, and send the corresponding photons into two optical fibers that are connected to two ultrafast superconducting-nanowire single photon detectors. $C_{1p,N}$ ($C_{1p,G}$) is centered on the normal (ghost) resonance of mode $1p$. The collection bandwidth is tuned to $\Gamma_{bw} \simeq 120\mu\text{eV}$, i.e. twice broader than $\hbar\gamma_{1p} \simeq 55\mu\text{eV}$, the spectral linewidth of mode $1p$, in order to achieve a good time resolution, while at the same time be able to separate spectrally the $1p$ mode from the other neighboring modes such as the $1d$ or the $1s$. Spatially, the positions of $C_{1p,N/G}$ are chosen to be centered on one of the antinodes of the $1p$ mode, so that about $\sim 20\%$ of the total spatial mode area is collected by the fibers and the two-photon coincidence rate $I_{NG}^{(2)}$ is maximal.

Such a measurement of $g_{NG,j}^{(2)}(\tau)$ is shown in Fig.2.c for a temperature $T = 4.2\text{K}$. It is obtained from the normal-ghost photon pairs coincidence counts $I_{NG}^{(2)}(\tau)$, where the delay τ between the two photons is measured with a $\sigma_\tau = 7.2\text{ ps}$ 1σ precision, and where $\tau > 0$ ($\tau < 0$) corresponds to events with the normal (ghost) photon being detected first. The normalization is obtained from

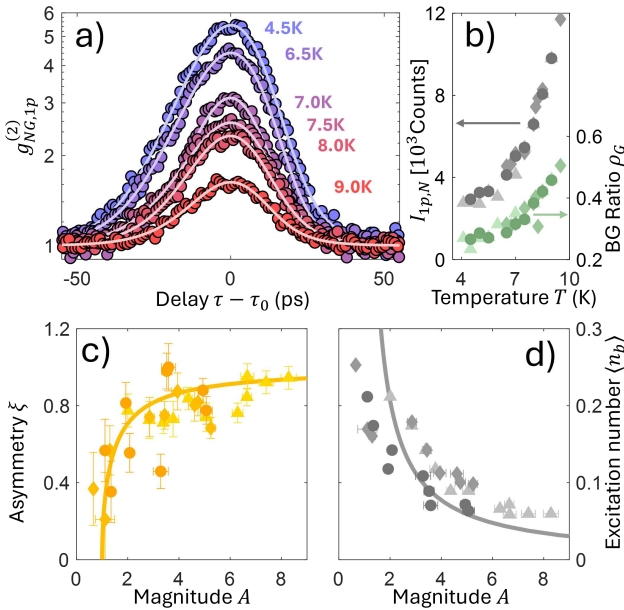


FIG. 3. **Correlation amplitude A and asymmetry ξ of the 1p Bogoliubov mode emission as a function of temperature T** – (a) Measurement of $g_{NG,1p}^{(2)}(\tau - \tau_0)$ as a function of the micropillar temperature (blue to red symbols for temperatures increasing from 4.4 K to 9 K). $\tau_0(\omega_{N,G}) \in [-15, 15]$ ps is a small unknown delay offset due to optical path length dependence on $\omega_{N,G}(T)$. The solid lines are fits to the data using the relaxed lineshape model. b) Measured emission intensity $I_{1p,N}$ of the normal 1p Bogoliubov mode (left axis), and proportion ρ_G of background emission at the 1p Ghost frequency (right axis), as a function of temperature. (c) Measured (symbols) correlation asymmetry ξ_M as a function of the measured correlation characteristic amplitude A_{Mc} , corrected from the uncorrelated background photons. The theoretical $\xi(A)$ is plotted as a solid line. (d) Measured (symbols) 1p number $n_{b,M}$ of Bogoliubov excitation as derived from (b) as a function of A_{Mc} . The theoretical $n_b(A)$ is plotted as a solid line. In (b,c,d), the three color shades and symbols (circles, diamonds, triangles) corresponds to three separate experimental runs, the data in (a) come from the first run.

the measured normal and ghost photon detection rates on each detectors. The max correlation exhibited by the data amounts to $g_{NG,1p,\max}^{(2)} = \max[g_{NG,1p}^{(2)}(\tau)] = 9.0 \pm 0.3$, way larger than 1 that would characterize uncorrelated pairs. The correlation peak exhibits also a strongly asymmetric shape (for visual assessment of the asymmetry, a symmetric lineshape matching the right side of the measured $g_{NG,1p}^{(2)}(\tau)$ is shown in Fig.2.c), that can be quantified by means of a fit using a relaxed lineshape model based on Eq.(6) where A and ξ are left as free independent parameters, i.e. without enforcing the relation Eq.(9) between them. All the fitting procedures includes the instrument finite time-resolution by means of a Gaussian convolution. This fit yields the measured parameters $A_M = 6.05 \pm 0.22$ and $\xi_M = 0.94 \pm 0.06$. This

latter value has the expected positive sign, corresponding to a leading ghost photon, and it is close to the maximal theoretical time-ordering value $\xi = 1$. This is a key signature of the particle and hole quantum superposition as explained earlier.

To verify the robustness of this feature, we examine if the measured asymmetry and characteristic amplitude A_M and ξ_M obey the relation of Eq.(9). If we apply Eq.(9) to the measured value A_M , we get $\xi(A_M) = 0.91 \pm 0.003$ which is fully consistent with the measured value $\xi_M = 0.94 \pm 0.06$. This value corresponds to an average number of Bogoliubov excitations $n_b \simeq 0.05$, showing that the 1p contribution to the total Bogoliubov fluctuation is indeed deep into the quantum regime, in which the \cup stochastic excursions are strongly suppressed.

We then take advantage of the fact that in our system, the Bogoliubov excitations are coupled to the thermal bath of solid-state photons [29], so that n_b can be increased by increasing the microcavity temperature. We thus measure $g_{NG,1p}^{(2)}(\tau)$ for temperatures increasing from 4.2 K to 10 K. Examples of such correlation functions are shown in Fig.3.a. The data exhibit the trend predicted by the theoretical $A(n_b)$ and $\xi(n_b)$ in Eqs.(8-7): for increasing temperature, $g_{NG,1p,\max}$ decreases significantly, while the asymmetry gets smaller.

To perform this analysis quantitatively and as accurately as possible, we account for the fact that in the actual experiment, the spectral tail of the lower 1s mode, as well as some unstructured background emission $I_{G,bg}$, contribute a fraction ρ_G of the total number of photons at the 1p Ghost frequency: the measured $\rho_G(T)$ is plotted in Fig.3.b (see SI section 1 for the measurement method). This unwanted emission results in the two following mild deviations (i,ii) from the ideal single-mode model that we can mitigate with a slightly more sophisticated analysis.

(i) Owing to the different spatial pattern of $I_{bg,G}$, the 1s, and the 1p mode, ρ_G leads to a smaller value of the measured correlation when the detection is shifted away from the anti-node of the 1p mode. Although we use microscopy to position $C_{1p,N,G}$ at one of 1p's antinode as accurately as possible, we repeat the measurement three times to be sure that the measured trend relating $A_M(T)$ and $\xi_M(T)$ is due to $n_b(T)$ as desired, and not to a spatial repositioning fluctuations in the detection.

(ii) A non-zero ρ_G means that not only 1p photons but also photons from other sources are both contributing to pair counts, a situation that deviates from the single mode case. Fortunately, the fraction of non-1p photons at the normal frequency amount to $\rho_N < 4\%$ in the interval $T = [4, 10]$ K (see SI section I for the measurement). As a result, the Ghost background photons only contribute accidental pairs with the Normal photons and ρ_G only leads to a correction of the normalization factor in $g_{NG,1p}^{(2)}(\tau)$ by a factor $(1 - \rho_G)^{-1}$. We can thus apply this correction to determine the 1p-only correlation amplitude in the measurement $A_{Mc} = A_M / (1 - \rho_G)$, while the measured asymmetry ξ_M needs no correction.

The data pairs $(A_{Mc}, \xi_M)[T]$ obtained in this way are plotted in Fig.3.c, alongside the theoretical prediction Eq.(9) for $A(\xi)$. A solid agreement is found between the two, confirming that the observed correlation parameters A and ξ are indeed consistent with Bogoliubov's time-ordering mechanism of the photons, in the regime $n_b < 1$, and over the explored range of $n_b(T)$.

Interestingly, we can determine a measurement of the $1p$ excitation number $n_{b,M}(T)$ independently from the correlation measurement, using the fact that $n_b(T) = K I_{1p,N}(T)$, where $I_{1p,N}(T)$ is the Bogoliubov emission intensity at the Normal $1p$ frequency, integrated over the narrow emission peak, and that within this temperature range, K is a single unknown constant. In Fig.3.d, we thus plot $(A_{Mc}, n_{b,M})[T]$ and determine K so to obtain the best fit with eq.(7). We obtain a reasonable agreement, which allows us to determine that n_b increases from $n_b \simeq 0.05$ at $T = 4\text{ K}$ to $n_b \simeq 0.25$ at $T = 10\text{ K}$. In all the considered range of temperatures, the system thus remains deep in the quantum regime.

DISCUSSION

In order to put our observations in a broader context, it is important to note that time-ordered two-photon correlations have been observed in previous works, but only in the emission from quantum two-level systems, in which the physical origin of time-ordering asymmetry is very different. Resonantly-driven two-level atoms, for instance, can exhibit time-ordering [35] in the cross-correlation between two photons from the opposite sidebands of a Mollow triplet. But this time ordering occurs when the driving frequency is detuned from the two-level dipole resonance, and it originates from the uneven weights of the photon and dipole components in the dressed eigenstates wavefunctions [7, 32, 36, 37]. In particular, the underlying Jaynes-Cumming ladder of these dressed excitations does not match at all – in nature and level spacing – that of our system.

Other cascading quantum systems can also exhibit time-ordering, like inverted three-level systems in, e.g., solid-state quantum dots [38]. Here, time-ordering emerges as a result of a cascading dynamics in the relaxation from level three to one, associated to a strong intrinsic nonlinearity due, e.g., to the biexciton Coulomb binding energy [39], that distinguishes the two transitions in frequency and/or polarization [38]. Interestingly, our system can also exhibit a cascading photons correlation under incoherent excitation driving a few intracavity photons [40], as a result of a weak blockade mechanism [41]. In principle, this regime can also generate time-ordered photons due to deexcitation down the anharmonic excitation ladder. However, a different timer-order correlation magnitude and characteristics would be expected, as in this different regime, the excitations nature is quite different from Bogoliubov's.

Finally, since the Bogoliubov framework is appropri-

ate for the description of spontaneous parametric emission in a quite broad class of systems [42], our time-ordering mechanism could also be in principle observed in non-polaritonic nonlinear microstructures. However, such systems have to involve at most two discrete modes within the spectral bandwidth of the nonlinearity, a condition which is usually not reached in broadband transparent systems like nonlinear waveguides or ring-resonators [43]. As soon as a triple resonance condition for parametric scattering is possible, the system involves at least two degenerate Bogoliubov modes of opposite Normal and ghost frequencies with respect to each other, and hence with suppressed time-ordering.

CONCLUSION

Weakly nonlinear photonic systems are much simpler to engineer and control than artificial two-level atoms, and have the potential to generate complex, interesting, and useful many-body quantum states of light. Exploring this physics is of high interest both in the context of quantum technologies and at a fundamental level. In this work, we have shown that the quantum superposition of creation and annihilation processes, which is fundamental to the nature of Bogoliubov excitations, drives time-ordered photon-pair correlations, that emerge and grow stronger upon getting deeper into the quantum regime of the fluctuations, i.e. for average values of the excitation number of the Bogoliubov field decreasing far below unity. This particular type of correlations, show that that Bogoliubov states of light have a richer quantum structure than originally pictured. The deterministic photon ordering could be used for instance to prepare pure states of time-ordering entanglement; and beyond the steady-state regime, one can also expect this ordering to have an effect on the flash of quantum light which is expected by a quench of the Bogoliubov vacuum [44]. These questions constitute important experimental and theoretical follow-up to this work.

ACKNOWLEDGEMENTS

MR, AB, FC and YZ acknowledge financial support from the Centre for Quantum technologies 'Exploratory Initiative program', and from the National Research Foundation via CNRS@CREATE internal grant 'NGAP'. IC acknowledges financial support from Provincia Autonoma di Trento (PAT); from the Q@TN Initiative; from the National Quantum Science and Technology Institute through the PNRR MUR project under Grant PE0000023-NQSTI, co-funded by the European Union – NextGeneration EU. SR, AB, AL and MM acknowledge support from the European Research Council under the European Union's Horizon 2020 research and innovation programme through the Grant ARQADIA (grant agreement no. 949730) and under the Horizon Europe

programme (project ANAPOLIS, grant agreement no. 101054448), by the RENATECH network and the General Council of Essonne, by the Paris Ile-de-France Région via DIM SIRTEQ and DIM QUANTIP, by the Plan France 2030 through the project QUTISYM ANR23-PETQ-0002, and by the ANR project Ngauge (ANR-24-CE92-0011). AB is member of the Institut Universitaire de France. MR wishes to thank Thomas Volz for stimulating discussions.

METHODS

A. Experimental system

The experiment is carried out on a single Arsenide-based solid-state micropillar microcavities of $7\ \mu\text{m}$ diameter. The micropillar exhibits discrete transverse modes of exciton-polaritons that result from the strong coupling regime between discrete laterally-confined cavity modes, and the excitonic transition of a single InGaAs quantum well placed at the longitudinal cavity mode antinode [45–47]. The polaritonic character is essential to provide an effective two-body interaction, which is large enough to contribute significantly within the intra-cavity lifetime, and low enough to place the system in the weakly interacting regime in which the Bogoliubov picture is valid.

B. Multimode theory of nonlinear a 0D micropillar microcavity

1. Polaritonic levels in the linear regime

Following an approach similar to that in [48], we can describe the conservative part of the system with the exciton-polariton Hamiltonian

$$\hat{H}_0 = \hbar \sum_j \left[\omega_{c,j} \hat{a}_j^\dagger \hat{a}_j + \omega_x \hat{b}_j^\dagger \hat{b}_j + \frac{\Omega}{2} (\hat{a}_j^\dagger \hat{b}_j + \hat{b}_j^\dagger \hat{a}_j) \right] + \hat{H}_V \quad (10)$$

where ω_x is the the excitonic transition frequency, Ω is the Rabi frequency coupling cavity photons and excitons, and $\omega_{c,j}$ is the cavity resonance of transverse mode j . The transverse modes \hat{a}_j in cylindrical micropillars of radius R ($R = 3.5\ \mu\text{m}$ for this micropillar) are described by the set of eigen-functions $\phi_{n,m}(r, \theta) = \sqrt{A_{n,m}} e^{im\theta} J_m(z_{n,m}r/R)$, where $\mathbf{r} = (r, \theta)$ are the spatial coordinate, $j = (n, m)$ are the radial and azimuthal numbers, $A_{n,m}$ is the normalization factor, $J_m(x)$ are Bessel the functions of order m , and $z_{n,m}$ is the n^{th} zero of $J_m(x)$. The transverse mode j thus reads $\hat{a}_j = \int_{r \leq R} d^2\mathbf{r} \phi_j(\mathbf{r}) \hat{a}(\mathbf{r})$ with $\hat{a}(\mathbf{r})$ the cavity-photon field at in-plane position $\mathbf{r} = (r, \theta)$. We define similarly $\hat{b}(\mathbf{r})$ the quantum well exciton field, that we also express in the Bessel function basis via the set of operators $\{\hat{b}_j\}$.

The Hamiltonian term $\hat{H}_V = \int_{r \leq R} d^2\mathbf{r} h_V(r) \hat{b}^\dagger(\mathbf{r}) \hat{b}(\mathbf{r})$, with $h_V(r) = -\hbar a_2(r/R)^2$ describes the excitonic potential within the micropillar, that we determined in a separate micro-spectroscopy analysis. This radial potential accounts for the crystalline strain relaxation at the micropillar edges. We can also express \hat{H}_V in the Bessel function basis. More specifically, we use the $N = 94$ first eigenstates of the bare photonic micropillar microcavity of radius R and refractive index n_0 , as the representation basis.

We thus obtain \hat{H}_0 in a (188×188) matrix form. Diagonalizing \hat{H}_0 provides the confined polariton levels and eigenstates (cf. modes levels and labels in Fig.2.a), that we can compare (both in terms of energy and cross-section amplitude), with the spatially-resolved measured spectra, like that in Fig.2.a. We can thus determine the parameters describing the system, namely: $\{\hbar\omega_x, \hbar\omega_{c0}, \hbar\Omega, \hbar a_2\} = \{1445.83 \pm 0.02, 1442.078 \pm 0.02, 3.47 \pm 0.02, 1.31 \pm 0.03\}$ meV, where ω_{c0} is the unconfined cavity mode frequency and $n_0 = 3.51 \pm 0.01$.

2. Polaritonic Bogoliubov levels

We add a coherent drive $\hat{H}_D = (F^* e^{i\omega_{\text{las}} t} \hat{a}_{j_0} + \text{h.c.})$ to \hat{H}_0 , where j_0 labels the driven mode (for the measurement in Fig.2.b, $\hbar\omega_{\text{las}} = 1441.85$ meV). We assume that the pump-induced nonlinearities have a negligible effect on the spatial structure of the driven mode. We then add the typical interaction terms known to be relevant to exciton-polaritons [49]: $\hat{V}_{xx} = (\hbar g_x/2) \int_{r \leq R} d^2\mathbf{r} \hat{b}^\dagger(\mathbf{r}) \hat{b}^\dagger(\mathbf{r}) \hat{b}(\mathbf{r}) \hat{b}(\mathbf{r})$ that describes exciton-mediated scattering, and $\hat{V}_{\text{sat}} = (-\hbar g_s/2) \int_{r \leq R} d^2\mathbf{r} [\hat{a}^\dagger(\mathbf{r}) \hat{b}^\dagger(\mathbf{r}) \hat{b}(\mathbf{r}) \hat{b}(\mathbf{r}) + \text{h.c.}]$ that describe an oscillator saturation mechanism. Our resonantly driven nonlinear micropillar microcavity is described by $\hat{H}_0 + \hat{H}_D + \hat{V}_{xx} + \hat{V}_{\text{sat}}$

To describe the Bogoliubov levels, we first derive the resonantly driven mode steady-state solution for the excitonic and photonic complex-valued mean-fields Ψ_x and Ψ_c . The losses are introduced in the equations in the usual way [31]. In a second step, we linearize the equations of motion around the mean-field solution (Bogoliubov approximation), and thus obtain the dynamics of the small (Bogoliubov) fluctuations. These equations of motions, including the losses, can be expressed in the basis described earlier in a matrix form as

$$\frac{\partial \hat{\mathbf{A}}}{\partial t} = M_B \hat{\mathbf{A}}, \quad (11)$$

where M_B is the Bogoliubov Matrix, and $\hat{\mathbf{A}} = [\hat{a}_1 \dots \hat{a}_N, \hat{b}_1 \dots \hat{b}_N, \hat{a}_1^\dagger \dots \hat{a}_N^\dagger, \hat{b}_1^\dagger \dots \hat{b}_N^\dagger]^T$ is a column vector of excitonic and photonic fluctuations operators where the index refers to the N elements of the Bessel function basis considered. The Bogoliubov levels are obtained by diagonalizing M_B .

Formally, the Bogoliubov eigenstates consists in linear superpositions of the polaritonic transverse states, however, since the energy scale of the nonlinear terms are comparable or smaller than the splitting between two consecutive states (such as $1s - 1p$ or $1p - 1d$), the Bogoliubov states remain dominated by a single eigenstate, and the labeling ($1s$, $1p$, $1d$) remains approximately valid. The resulting levels and labeling, obtained from fitting this model to the measured Bogoliubov spec-

trum is shown in Fig.2.b. The fitting parameters are the two characteristic nonlinear energies $g_s|\Psi_x|^2 \simeq 0.7 \text{ meV}$ and $g_{xx}|\Psi_x|^2 \simeq 0.0 \text{ meV}$. Note that the negligible value of the latter is consistent with previous observations in an unconfined 2D geometry [49], but due to the larger uncertainties on ω_x and to the quadratic approximation for H_V that are specific of the micropillar microcavity system, a quantitative analysis of the ratio of g_{xx} and g_s would require a dedicated experimental work which is beyond the scope of this work.

[1] R. HANBURY BROWN and R. Q. TWISS, A test of a new type of stellar interferometer on sirius, *Nature* **178**, 1046 (1956).

[2] C. K. Hong, Z. Y. Ou, and L. Mandel, Measurement of subpicosecond time intervals between two photons by interference, *Phys. Rev. Lett.* **59**, 2044 (1987).

[3] T. Wilk, S. C. Webster, A. Kuhn, and G. Rempe, Single-atom single-photon quantum interface, *Science* **317**, 488 (2007).

[4] P. Senellart, G. Solomon, and A. White, High-performance semiconductor quantum-dot single-photon sources, *Nature Nanotechnology* **12**, 1026 (2017).

[5] A. Blais, S. M. Girvin, and W. D. Oliver, Quantum information processing and quantum optics with circuit quantum electrodynamics, *Nature Physics* **16**, 247 (2020).

[6] T. Heindel, J.-H. Kim, N. Gregersen, A. Rastelli, and S. Reitzenstein, Quantum dots for photonic quantum information technology, *Adv. Opt. Photon.* **15**, 613 (2023).

[7] B. L. Ng, C. H. Chow, and C. Kurtsiefer, Observation of the mollow triplet from an optically confined single atom, *Phys. Rev. A* **106**, 063719 (2022).

[8] M. Greiner, O. Mandel, T. Esslinger, T. W. Hänsch, and I. Bloch, Quantum phase transition from a superfluid to a mott insulator in a gas of ultracold atoms, *Nature* **415**, 39 (2002).

[9] A. Minguzzi and D. M. Gangardt, Exact coherent states of a harmonically confined tonks-girardeau gas, *Phys. Rev. Lett.* **94**, 240404 (2005).

[10] D. E. Chang, V. Gritsev, G. Morigi, V. Vuletić, M. D. Lukin, and E. A. Demler, Crystallization of strongly interacting photons in a nonlinear optical fibre, *Nature Physics* **4**, 884 (2008).

[11] I. Carusotto, D. Gerace, H. E. Tureci, S. De Liberato, C. Ciuti, and A. Imamoğlu, Fermionized photons in an array of driven dissipative nonlinear cavities, *Phys. Rev. Lett.* **103**, 033601 (2009).

[12] J. M. Wilson, N. Malvania, Y. Le, Y. Zhang, M. Rigol, and D. S. Weiss, Observation of dynamical fermionization, *Science* **367**, 1461 (2020).

[13] J. C. B. Paredes, P. Zoller, Fractional quantum hall regime of a gas of ultracold atoms, *Solid State Comm.* **127**, 155 (2003).

[14] N. Regnault and T. Jolicoeur, Quantum hall fractions in rotating bose-einstein condensates, *Phys. Rev. Lett.* **91**, 030402 (2003).

[15] J. Léonard, S. Kim, J. Kwan, P. Segura, F. Grusdt, C. Repellin, N. Goldman, and M. Greiner, Realization of a fractional quantum hall state with ultracold atoms, *Nature* **619**, 495 (2023).

[16] A. S. Sørensen, E. Demler, and M. D. Lukin, Fractional quantum hall states of atoms in optical lattices, *Phys. Rev. Lett.* **94**, 086803 (2005).

[17] J. Cho, D. G. Angelakis, and S. Bose, Fractional quantum hall state in coupled cavities, *Phys. Rev. Lett.* **101**, 246809 (2008).

[18] R. O. Umucalilar and I. Carusotto, Fractional quantum hall states of photons in an array of dissipative coupled cavities, *Phys. Rev. Lett.* **108**, 206809 (2012).

[19] L. W. Clark, N. Schine, C. Baum, N. Jia, and J. Simon, Observation of Laughlin states made of light, *Nature* **582**, 41 (2020).

[20] N. Bogoliubov, On the theory of superfluidity, *J. Phys. USSR* **11**, 23 (1947).

[21] L. Pitaevskii and S. Stringari, *Bose-Einstein Condensation and Superfluidity*, International series of monographs on physics (Oxford University Press, 2016).

[22] J. Steinhauer, R. Ozeri, N. Katz, and N. Davidson, Excitation spectrum of a Bose-Einstein condensate, *Phys. Rev. Lett.* **88**, 120407 (2002).

[23] A. Amo, J. Lefrère, S. Pigeon, C. Adrados, C. Ciuti, I. Carusotto, R. Houdré, E. Giacobino, and A. Bramati, Superfluidity of polaritons in semiconductor microcavities, *Nature Physics* **5**, 805 (2009).

[24] R. Lopes, C. Eigen, N. Navon, D. Clément, R. P. Smith, and Z. Hadzibabic, Quantum depletion of a homogeneous bose-einstein condensate, *Phys. Rev. Lett.* **119**, 190404 (2017).

[25] J. M. Vogels, K. Xu, C. Raman, J. R. Abo-Shaeer, and W. Ketterle, Experimental observation of the Bogoliubov transformation for a Bose-Einstein condensed gas, *Phys. Rev. Lett.* **88**, 060402 (2002).

[26] J. M. Zajac and W. Langbein, Parametric scattering of microcavity polaritons into ghost branches, *Phys. Rev. B* **92**, 165305 (2015).

[27] Q. Fontaine, T. Bienaimé, S. Pigeon, E. Giacobino, A. Bramati, and Q. Glorieux, Observation of the Bogoliubov dispersion in a fluid of light, *Phys. Rev. Lett.* **121**, 183604 (2018).

[28] F. Claude, M. J. Jacquet, R. Usciat, I. Carusotto, E. Giacobino, A. Bramati, and Q. Glorieux, High-resolution coherent probe spectroscopy of a polariton quantum fluid, *Phys. Rev. Lett.* **129**, 103601 (2022).

[29] I. Frérot, A. Vashisht, M. Morassi, A. Lemaître, S. Ravets, J. Bloch, A. Minguzzi, and M. Richard, Bogoliubov excitations driven by thermal lattice phonons in a quantum fluid of light, *Phys. Rev. X* **13**, 041058 (2023).

[30] A. Tenart, G. Hercé, J.-P. Bureik, A. Dureau, and D. Clé-

ment, Observation of pairs of atoms at opposite momenta in an equilibrium interacting bose gas, *Nature Physics* **17**, 1364 (2021).

[31] I. Carusotto and C. Ciuti, Quantum fluids of light, *Rev. Mod. Phys.* **85**, 299 (2013).

[32] E. del Valle, A. Gonzalez-Tudela, F. P. Laussy, C. Tejedor, and M. J. Hartmann, Theory of frequency-filtered and time-resolved n -photon correlations, *Phys. Rev. Lett.* **109**, 183601 (2012).

[33] X. Busch, I. Carusotto, and R. Parentani, Spectrum and entanglement of phonons in quantum fluids of light, *Phys. Rev. A* **89**, 043819 (2014).

[34] P. Stepanov, I. Amelio, J. G. Rousset, J. Bloch, A. Lemaître, A. Amo, A. Minguzzi, I. Carusotto, and M. Richard, Dispersion relation of the collective excitations in a resonantly driven polariton fluid, *Nature Communications* **10**, 3869 (2019).

[35] A. Aspect, G. Roger, S. Reynaud, J. Dalibard, and C. Cohen-Tannoudji, Time correlations between the two sidebands of the resonance fluorescence triplet, *Phys. Rev. Lett.* **45**, 617 (1980).

[36] G. Nienhuis, Spectral correlations in resonance fluorescence, *Phys. Rev. A* **47**, 510 (1993).

[37] A. Ulhaq, S. Weiler, S. M. Ulrich, R. Roßbach, M. Jetter, and P. Michler, Cascaded single-photon emission from the mollow triplet sidebands of a quantum dot, *Nature Photonics* **6**, 238 (2012).

[38] E. Moreau, I. Robert, L. Manin, V. Thierry-Mieg, J. M. Gérard, and I. Abram, Quantum cascade of photons in semiconductor quantum dots, *Phys. Rev. Lett.* **87**, 183601 (2001).

[39] Y. Z. Hu, S. W. Koch, M. Lindberg, N. Peyghambarian, E. L. Pollock, and F. F. Abraham, Biexcitons in semiconductor quantum dots, *Phys. Rev. Lett.* **64**, 1805 (1990).

[40] L. Scarpelli, C. Elouard, M. Johnsson, M. Morassi, A. Lemaître, I. Carusotto, J. Bloch, S. Ravets, M. Richard, and T. Volz, Probing many-body correlations using quantum-cascade correlation spectroscopy, *Nature Physics* **20**, 214 (2024).

[41] G. Munoz-Matutano, A. Wood, M. Johnsson, X. Vidal, B. Q. Baragiola, A. Reinhard, A. Lemaître, J. Bloch, A. Amo, G. Nogues, B. Besga, M. Richard, and T. Volz, Emergence of quantum correlations from interacting fibre-cavity polaritons, *Nature Materials* **18**, 213 (2019).

[42] S. L. Braunstein, Squeezing as an irreducible resource, *Phys. Rev. A* **71**, 055801 (2005).

[43] D. Zhu, L. Shao, M. Yu, R. Cheng, B. Desiatov, C. J. Xin, Y. Hu, J. Holzgrafe, S. Ghosh, A. Shams-Ansari, E. Puma, N. Sinclair, C. Reimer, M. Zhang, and M. Lončar, Integrated photonics on thin-film lithium niobate, *Adv. Opt. Photon.* **13**, 242 (2021).

[44] S. Koghee and M. Wouters, Dynamical casimir emission from polariton condensates, *Phys. Rev. Lett.* **112**, 036406 (2014).

[45] J. Bloch, R. Planel, V. Thierry-Mieg, J. Gérard, D. Barrier, J. Marzin, and E. Costard, Strong-coupling regime in pillar semiconductor microcavities, *Superlattices and Microstructures* **22**, 371 (1997).

[46] T. Gutbrod, M. Bayer, A. Forchel, J. P. Reithmaier, T. L. Reinecke, S. Rudin, and P. A. Knipp, Weak and strong coupling of photons and excitons in photonic dots, *Phys. Rev. B* **57**, 9950 (1998).

[47] O. El Daif, A. Baas, T. Guillet, J.-P. Brantut, R. I. Kaitouni, J. L. Staehli, F. Morier-Genoud, and B. Deveaud, Polariton quantum boxes in semiconductor microcavities, *Applied Physics Letters* **88**, 061105 (2006).

[48] R. I. Kaitouni, O. El Daif, A. Baas, M. Richard, T. Paraiso, P. Lugan, T. Guillet, F. Morier-Genoud, J. D. Ganière, J. L. Staehli, V. Savona, and B. Deveaud, Engineering the spatial confinement of exciton polaritons in semiconductors, *Phys. Rev. B* **74**, 155311 (2006).

[49] M. Richard, I. Frérot, S. Ravets, J. Bloch, C. Anton-Solanas, F. Claude, Y. Zhou, M. Morassi, A. Lemaître, I. Carusotto, , and A. Minguzzi, *Excitonic oscillator-strength saturation dominates polariton-polariton interactions* (2025), arXiv:2501.07899 [cond-mat.mes-hall].

SUPPLEMENTAL MATERIAL: Pairs of time-ordered photons from a single polaritonic Bogoliubov mode

I. ESTIMATION OF THE BACKGROUND PHOTONS FRACTION AT THE NORMAL AND GHOST $1p$ BOGOLIUBOV FREQUENCIES

The background contribution $\rho_{G,N}$ is determined from the measured spatially-resolved spectra $I_{\omega,x}$ such as the one shown in Fig.2.b of the main text, or the one shown in Fig.S1.a ($T = 4\text{ K}$) as follows. We extract A cross-section spectrum $I_c(\omega)$, spatially centered on one of the two spatial antinode of the $1p$ mode, and over a spatial width which is comparable with that collected by the fiber (cf. dashed white line in Fig.S1.a). The thus obtained spectra are shown in Fig.S1.(b-c) in the vicinity of the Ghost ($I_{c,G}(\omega)$) and Normal ($I_{c,N}(\omega)$) resonance respectively.

Each spectrum consists in a well-defined and well-identified peak corresponding to the $1p$ Bogoliubov resonance $I_{1p;N,G}$, on top of a slowly varying background $I_{BG;N,G}$ due to the spectral tail of the Bogoliubov $1s$ -mode photons, and to a broad background probably due to bare electron-hole emission occurring around the bare exciton level. these spectra are fitted using $I_{f;N,G}(\omega) = I_{1p;N,G}(\omega) + I_{BG;N,G}(\omega)$ where a known Voigt lineshape is used for the Bogoliubov peak, and an off resonant shallow broad peak is used for the Background. The result with the different contributions is shown in Fig.S1.(b-c). The background contribution $\rho_{N,G}$ is then determined as $\rho_{N,G} = \sum_{j \in \Delta_{N,G}} I_{BG;N,G}(\omega_j) / (I_{1p;N,G}(\omega_j) + I_{BG;N,G}(\omega_j))$, and the sum runs over an interval $\Delta_{N,G} = \omega_{1p,N,G} \pm 2.5\gamma_{1p,N,G}$ centered on the Bogoliubov peak resonance $\omega_{1p,N,G}$ and extends over $2.5 \times$ the resonance linewidth $\gamma_{1p;N,G}$.

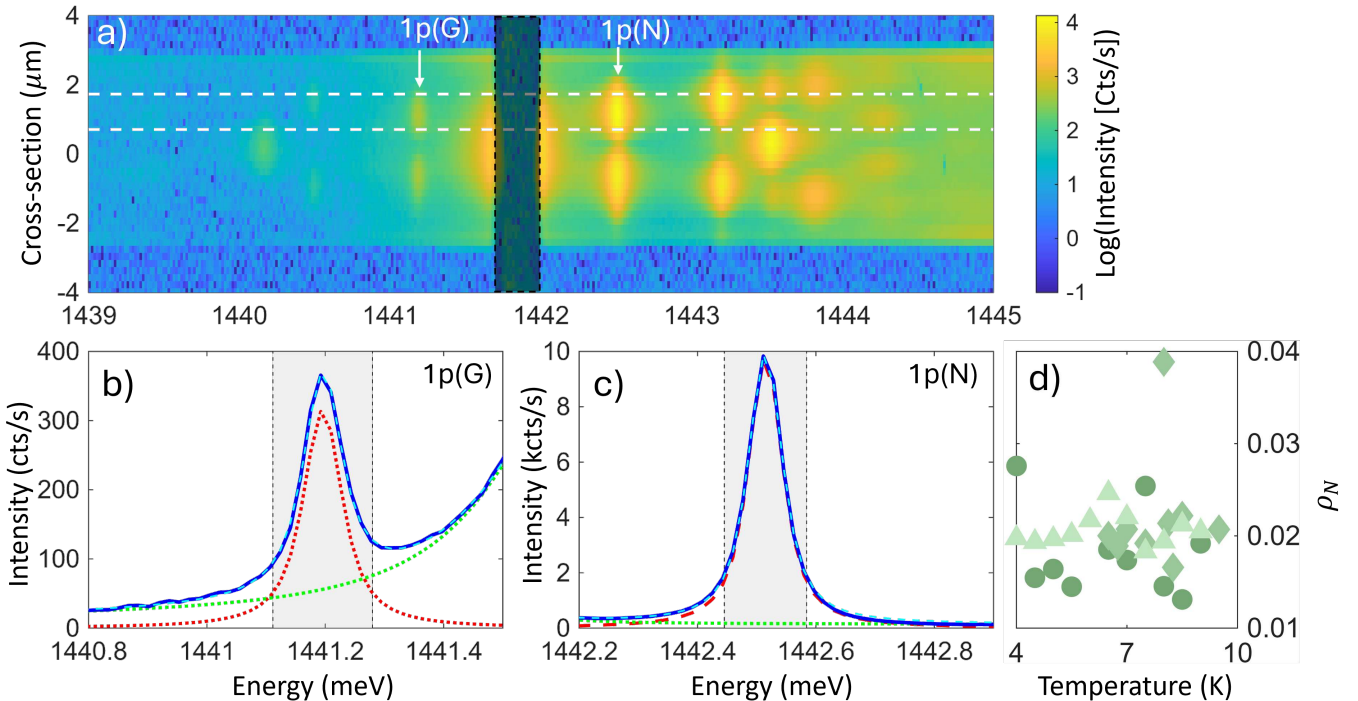


FIG. S1. a) Spatially-resolved Bogoliubov emission spectrum $I(\omega, x)$ in Color Log scale. The Normal and Ghost $1p$ Bogoliubov resonances '1p(N)' and '1p(G)', are indicated. The horizontal dashed line show the width of the spatial integration for the extracted cross-section spectrum $I_c(\omega)$. $I_{c,G}$ and $I_{c,N}$ show details of $I_c(\omega)$ focused on the Ghost (b) and Normal (c) resonances respectively (blue solid line). The fitted spectra $I_{f;N,G}$ are shown as cyan dashed line. They consist in a sum of the background contribution $I_{BG;N,G}(\omega)$ (green dotted line) and of the $1p$ Bogoliubov photons $I_{1p;N,G}(\omega)$ (red dotted line). The gray area, indicates the bandwidth in which the ratio $\rho_{G,N}$ is calculated. d) ρ_N for the 3 experimental runs using the same conventions as in main text Fig.3.b.

II. DERIVATION OF $g^{(2)}(\tau)$ IN THE INPUT-OUTPUT SINGLE-MODE PICTURE

Assuming a system with a single discrete Bogoliubov mode, we have established in the main text that the coincidence rate between two photons of frequencies ω_s and $\omega_{s'}$, as measured after the two filters of equal bandwidth $\Gamma_s = \Gamma_{s'} = \Gamma_{bw}$, can be expressed as (Eq.(5) of the main text)

$$I_{s,s'}^{(2)}(\tau) = \left\langle \mathcal{T}_-[\hat{\alpha}_s^\dagger(T)\hat{\alpha}_{s'}^\dagger(T+\tau)]\mathcal{T}_+[\hat{\alpha}_{s'}(T+\tau)\hat{\alpha}_s(T)] \right\rangle, \quad (1)$$

where $\hat{\alpha}_s(\tau) = \hat{\alpha}_{in}(\tau) - i\sqrt{\kappa} \int_{-\infty}^{\tau} dt f_s(\tau-t) \hat{a}(t)$, κ is the intracavity field decay rate, and $f_s(t) = e^{-i\omega_s t} e^{-\Gamma_{bw} t}$ is the filter transmission function in the time domain. $\hat{\alpha}_{in}(\tau)$ describes the input quantum fluctuation field which is in the vacuum state. \mathcal{T}_\pm denotes time ordering (resp. negative time ordering) for the particle operator $\hat{a}(t)$. In the experimental condition of steady-state, the expression does not depend on the time T , and hence we have:

$$I_{s,s'}^{(2)}(\tau) \propto \int_{-\infty}^0 dt_1 f_s(-t_1) \int_{-\infty}^0 dt_2 f_s^*(-t_2) \int_{-\infty}^{\tau} dt'_1 f_{s'}(\tau-t'_1) \int_{-\infty}^{\tau} dt'_2 f_{s'}^*(\tau-t'_2) \langle \mathcal{T}_-[\hat{a}^\dagger(t_2)\hat{a}^\dagger(t'_2)]\mathcal{T}_+[\hat{a}(t'_1)\hat{a}(t_1)] \rangle \quad (2)$$

Assuming that we are only dealing with gaussian quantum states, we can use Wick's theorem, which leads to:

$$\begin{aligned} \langle \mathcal{T}_-[\hat{a}^\dagger(t_2)\hat{a}^\dagger(t'_2)]\mathcal{T}_+[\hat{a}(t'_1)\hat{a}(t_1)] \rangle &= \langle \hat{a}^\dagger(t_2)\hat{a}(t_1) \rangle \langle \hat{a}^\dagger(t'_2)\hat{a}(t'_1) \rangle \\ &+ \langle \hat{a}^\dagger(t_2)\hat{a}(t'_1) \rangle \langle \hat{a}^\dagger(t'_2)\hat{a}(t_1) \rangle \\ &+ \langle \mathcal{T}_-[\hat{a}^\dagger(t_2)\hat{a}^\dagger(t'_2)] \rangle \langle \mathcal{T}_+[\hat{a}(t'_1)\hat{a}(t_1)] \rangle. \end{aligned} \quad (3)$$

We see that the fundamental building blocks of the expression for $I_{s,s'}^{(2)}$ are the particle correlations $\langle \hat{a}^\dagger(t)\hat{a}(t') \rangle$ and $\langle \hat{a}(t)\hat{a}(t') \rangle$. We evaluate them thereafter. First, we introduce the quantities:

$$g_{s,s'}(\tau) = \langle \hat{\alpha}_{s'}^\dagger(\tau)\hat{\alpha}_s(0) \rangle \quad (4)$$

$$I_s = g_{s,s}(0) \quad (5)$$

$$h_{s,s'}(\tau) = \langle \mathcal{T}_+[\hat{\alpha}_{s'}(\tau)\hat{\alpha}_s(0)] \rangle \quad (6)$$

Notice that time ordering appears in $h_{s,s'}$ but not in $g_{s,s'}$. Then we have:

$$I_{s,s'}^{(2)}(\tau) = I_s I_{s'} + |g_{s,s'}(\tau)|^2 + |h_{s,s'}(\tau)|^2 \quad (7)$$

and for $g^{(2)}$:

$$g_{s,s'}^{(2)}(\tau) = \frac{I_{s,s'}^{(2)}(\tau)}{I_s I_{s'}} = 1 + \frac{|g_{s,s'}(\tau)|^2 + |h_{s,s'}(\tau)|^2}{I_s I_{s'}} \quad (8)$$

Photon correlations.— We then evaluate polariton correlations. We introduce the quantities:

$$g(\tau) = \langle \hat{a}^\dagger(\tau)\hat{a}(0) \rangle \quad (9)$$

$$h(\tau) = \langle \hat{a}(\tau)\hat{a}(0) \rangle \quad (10)$$

Throughout the calculation, we assume that $\langle \hat{\beta}^\dagger \hat{\beta} \rangle = 0$. This approximation can be well justified in the limit where $\omega_0 \gg \gamma$ when adding a dissipative term coupled to the photon operator \hat{a} . We also introduce a finite linewidth γ to the mode at frequency ω_0 . Using $\hat{a}(t) = [u\hat{\beta}e^{-i\omega_0 t} + v\hat{\beta}^\dagger e^{i\omega_0 t}]e^{-\gamma t}$, we find for $\tau \geq 0$:

$$g(\tau) = e^{-\gamma\tau} [u^2 \langle \hat{\beta}^\dagger \hat{\beta} \rangle e^{i\omega_0 \tau} + v^2 \langle \hat{\beta} \hat{\beta}^\dagger \rangle e^{-i\omega_0 \tau}] \quad (11)$$

$$h(\tau) = u v e^{-\gamma\tau} [\langle \hat{\beta}^\dagger \hat{\beta} \rangle e^{i\omega_0 \tau} + \langle \hat{\beta} \hat{\beta}^\dagger \rangle e^{-i\omega_0 \tau}] \quad (12)$$

Notice that we have $g(-\tau) = [g(\tau)]^*$, and that we do not need $h(-\tau)$ due to the time ordering in evaluating $h_{s,s'}(\tau)$.

Detectors correlations.— We now sketch the computation for $h_{s,s'}(\tau)$:

$$h_{s,s'}(\tau) = \int_{-\infty}^0 dt f_s(-t) \int_{-\infty}^{\tau} dt' f_{s'}(\tau - t') \langle \mathcal{T}_+ [\hat{a}(t') \hat{a}(t)] \rangle \quad (13)$$

$$= \int_{-\infty}^0 dt f_s(-t) \left(\int_t^{\tau} dt' f_{s'}(\tau - t') \langle \hat{a}(t') \hat{a}(t) \rangle + \int_{-\infty}^t dt' f_{s'}(\tau - t') \langle \hat{a}(t) \hat{a}(t') \rangle \right) \quad (14)$$

$$= \int_{-\infty}^0 dt f_s(-t) \left(\int_t^{\tau} dt' f_{s'}(\tau - t') h(t' - t) + \int_{-\infty}^t dt' f_{s'}(\tau - t') h(t - t') \right) \quad (15)$$

We notice that $h(t)$ is a sum of terms with temporal dependence $e^{(\pm i\omega_0 - \gamma)\tau}$, and that $f_s(t) = e^{-i\omega_s t} e^{-\Gamma t}$. Evaluating $h_{s,s'}(\tau)$ is then a straightforward exercise of integrating exponential functions. In particular, a term $e^{(i\omega_0 - \gamma)\tau}$ in $h(\tau)$ gives for $h_{s,s'}(\tau)$ a contribution:

$$h_{s,s'}^{(\text{term } +\omega_0)}(\tau) = \frac{e^{-\Gamma\tau} e^{-i\omega_{s'}\tau}}{2\Gamma + i\omega_s + i\omega_{s'}} \left[\frac{1}{\Gamma + \gamma + i\omega_{s'} - i\omega_0} - \frac{1}{\Gamma - \gamma + i\omega_{s'} + i\omega_0} \right] \\ + \frac{e^{-\gamma\tau} e^{i\omega_0\tau}}{(\Gamma - \gamma + i\omega_{s'} + i\omega_0)(\Gamma + \gamma + i\omega_s - i\omega_0)} \quad (16)$$

Therefore, gathering both $e^{\pm i\omega_0}$ contributions, the final result for $h_{s,s'}(\tau)$ reads:

$$h_{s,s'}(\tau) = e^{-\Gamma\tau} e^{-i\omega_{s'}\tau} \frac{uv}{2\Gamma + i\omega_s + i\omega_{s'}} \left[\langle \hat{\beta}^\dagger \hat{\beta} \rangle \left(\frac{1}{\Gamma + \gamma + i\omega_{s'} - i\omega_0} - \frac{1}{\Gamma - \gamma + i\omega_0 + i\omega_{s'}} \right) \right. \\ \left. + \langle \hat{\beta} \hat{\beta}^\dagger \rangle \left(\frac{1}{\Gamma + \gamma + i\omega_0 + i\omega_{s'}} - \frac{1}{\Gamma - \gamma - i\omega_0 + i\omega_{s'}} \right) \right] \\ + e^{-\gamma\tau} e^{i\omega_0\tau} \frac{uv \langle \hat{\beta}^\dagger \hat{\beta} \rangle}{(\Gamma - \gamma + i\omega_0 + i\omega_{s'})(\Gamma + \gamma - i\omega_0 + i\omega_s)} \\ + e^{-\gamma\tau} e^{-i\omega_0\tau} \frac{uv \langle \hat{\beta} \hat{\beta}^\dagger \rangle}{(\Gamma - \gamma - i\omega_0 + i\omega_{s'})(\Gamma + \gamma + i\omega_0 + i\omega_s)} \quad (17)$$

Similarly, for $g_{s,s'}(\tau) = \int_{-\infty}^0 dt f_s(-t) \int_{-\infty}^{\tau} dt' f_{s'}^*(\tau - t') \langle \hat{a}^\dagger(t') \hat{a}(t) \rangle$, the final result reads:

$$g_{s,s'}(\tau) = e^{-\Gamma\tau} e^{-i\omega_{s'}\tau} \frac{1}{2\Gamma + i\omega_s - i\omega_{s'}} \left[u^2 \langle \hat{\beta}^\dagger \hat{\beta} \rangle \left(\frac{1}{\Gamma + \gamma + i\omega_0 - i\omega_{s'}} - \frac{1}{\Gamma - \gamma + i\omega_0 - i\omega_{s'}} \right) \right. \\ \left. + v^2 \langle \hat{\beta} \hat{\beta}^\dagger \rangle \left(\frac{1}{\Gamma + \gamma - i\omega_0 - i\omega_{s'}} - \frac{1}{\Gamma - \gamma - i\omega_0 - i\omega_{s'}} \right) \right] \\ + e^{-\gamma\tau} e^{i\omega_0\tau} \frac{u^2 \langle \hat{\beta}^\dagger \hat{\beta} \rangle}{(\Gamma - \gamma + i\omega_0 - i\omega_{s'})(\Gamma + \gamma - i\omega_0 + i\omega_s)} \\ + e^{-\gamma\tau} e^{-i\omega_0\tau} \frac{v^2 \langle \hat{\beta} \hat{\beta}^\dagger \rangle}{(\Gamma - \gamma - i\omega_0 - i\omega_{s'})(\Gamma + \gamma + i\omega_0 + i\omega_s)} \quad (18)$$

We then evaluate these expressions at resonance for N/G or G/N correlations, namely when $\omega_s = -\omega_{s'} = \pm\omega_0$. We establish approximate expressions by assuming that $\omega_0 \gg \gamma, \Gamma$, and keeping only the dominant term. We find:

$$h_{N,G}(\tau) = uv e^{i\omega_0\tau} \left[e^{-\Gamma\tau} \frac{1}{2\Gamma} \left(-\frac{\langle \hat{\beta}^\dagger \hat{\beta} \rangle}{\Gamma - \gamma} + \frac{\langle \hat{\beta} \hat{\beta}^\dagger \rangle}{\Gamma + \gamma} \right) + e^{-\gamma\tau} \frac{\langle \hat{\beta}^\dagger \hat{\beta} \rangle}{(\Gamma - \gamma)(\Gamma + \gamma)} \right] \quad (19)$$

$$h_{G,N}(\tau) = uv e^{-i\omega_0\tau} \left[e^{-\Gamma\tau} \frac{1}{2\Gamma} \left(\frac{\langle \hat{\beta}^\dagger \hat{\beta} \rangle}{\Gamma + \gamma} - \frac{\langle \hat{\beta} \hat{\beta}^\dagger \rangle}{\Gamma - \gamma} \right) + e^{-\gamma\tau} \frac{\langle \hat{\beta} \hat{\beta}^\dagger \rangle}{(\Gamma - \gamma)(\Gamma + \gamma)} \right] \quad (20)$$

We further notice that $g_{N,G}(\tau), g_{G,N}(\tau) \sim \mathcal{O}(1/(\gamma\omega_0))$, hence $|g_{s,s'}|^2 \ll |h_{s,s'}|^2$ for N/G and G/N correlations evaluated at the peak frequencies. Hence, in this limit we have the approximate expression:

$$g_{s,s'}^{(2)}(\tau) = 1 + \frac{|h_{s,s'}(\tau)|^2}{I_s I_{s'}} \quad (21)$$

Evaluating $I_s = g_{s,s}(0)$, we find in the limit $\omega_0 \gg \gamma, \Gamma$:

$$I_N = g_{N,N}(0) = \frac{u^2 \langle \hat{\beta}^\dagger \hat{\beta} \rangle}{\Gamma(\Gamma + \gamma)} \quad (22)$$

$$I_G = g_{G,G}(0) = \frac{v^2 \langle \hat{\beta} \hat{\beta}^\dagger \rangle}{\Gamma(\Gamma + \gamma)} \quad (23)$$

We obtain the final expression for $g^{(2)}$, valid in the limit $\omega_0 \gg \gamma, \Gamma$, and for the filter frequencies $\omega_s, \omega_{s'}$ centered on the peak frequency $\pm \omega_0$:

$$g_{N,G}^{(2)}(\tau) = 1 + \frac{\langle \hat{\beta}^\dagger \hat{\beta} \rangle}{\langle \hat{\beta} \hat{\beta}^\dagger \rangle} \frac{\Gamma^2}{(\Gamma - \gamma)^2} \left[e^{-\gamma\tau} - \frac{e^{-\Gamma\tau}}{2\Gamma \langle \hat{\beta}^\dagger \hat{\beta} \rangle} (\gamma - \Gamma + 2\gamma \langle \hat{\beta}^\dagger \hat{\beta} \rangle) \right]^2 \quad (24)$$

$$g_{G,N}^{(2)}(\tau) = 1 + \frac{\langle \hat{\beta} \hat{\beta}^\dagger \rangle}{\langle \hat{\beta}^\dagger \hat{\beta} \rangle} \frac{\Gamma^2}{(\Gamma - \gamma)^2} \left[e^{-\gamma\tau} - \frac{e^{-\Gamma\tau}}{2\Gamma \langle \hat{\beta} \hat{\beta}^\dagger \rangle} (\Gamma - \gamma + 2\gamma \langle \hat{\beta} \hat{\beta}^\dagger \rangle) \right]^2 \quad (25)$$

These expressions are equivalent to Eqs. (6-8) in the main text.